Chapter 3

Spectral characteristics of 6 MV Photon beam using the BEAMnrc code

ABSTRACT

The Monte Carlo (MC) methods are computational tools established as most dependable and precise methods for the analysis of radiation beam characteristics. In this chapter we have developed an accurate MC simulation model for 6 MV photon beam produced by Varian Clinic 600 linear accelerator (unique performance model) available at our Institute. We used this simulation model to calculate depth-dose profiles and the contribution of contaminant electron to it as with traditional methods of measurements; it is difficult to compute the dose delivered by different type of particles present in the radiation beam. We also evaluated the spectral characteristics of radiation beam by computing photon fluence spectra, photon average energy distributions, photon energy fluence spectra and contaminant electron fluence spectra. The computed data obtained from our simulation model were compared with the experimentally measured depth-dose and this data agreed within 1% of local dose, and 1.0 mm in depth for all depths and field sizes. It gave enough confidence that MC simulations could be used to simulate the 6 MV photon beam. Our results obtained from simulations showed that the contribution of electrons to the central-axis depth-dose was less than 7% of maximum total dose at surface, while at the depth of maximum dose (d_{max}) its contribution was less than 3% of maximum total dose for 10×10 cm^2 field sizes. The photon energy fluence spectra were separated into direct and scatter components from the primary collimator, flattening filter and the adjustable collimators. The contribution of direct photons to the total photon energy fluence was observed to be nearly 97% and the scatter contributions to the total photon energy fluence from the primary collimator and flattening filter were found to be typically less than 3% and scatter contributions from jaws was less than 0.30 % to the total photon energy fluence for a field size of 10×10 cm^2. Our study

showed that both photon and electron fluence spectra strongly depend upon field size. Most of the scatter energy fluence of photon comes from flattening filter and primary collimator. Beam hardening effect of flattening filter has also been verified in our study by the investigation of average energy distribution.

3.1 INTRODUCTION

The algorithms which are presently used in many commercially available treatment planning systems are of limited accuracy due to the implementation of many types of approximations in them for dose calculations. Therefore, in recent past the use of Monte Carlo (MC) methods have increased extensively for the benchmarking of photon and electron dose calculations in radiotherapy **[Sheu *et al.* (2006), Verhaegen *et al.* (2003), Ma *et al.* (1999), Sheikh-Bagheri *et.al* (2000)].** The application of the Monte Carlo methods in radiotherapy was initially proposed by Mackie and Battista **[Mackie *et al* (1984)],** since than MC method applications have been applied in numerous areas of radiotherapy such as radiation dosimetry, treatment machines, and treatment planning computations **[Sheikh-Bagheri *et al* (2002), Sheikh-Bagheri *et al* (2002), Verhaegen *et al* (2003), Mesbahi *et al* (2005), Mesbahi *et al* (2005), Mesbahi *et al* (2006), Mesbahi *et al* (2006), Farajollahi *et al* (2006), Mesbahi *et al* (2006)]**. These tools offer a very efficient and influential way of determining the effect of various components in linac head on dosimetric characteristics of radiation beam. With the development of faster computational systems, MC simulation offer an exclusive opportunity for their use in radiation oncology **[Fragoso *et al* (2009), Hasenbalg *et al* (2008), Rogers *et al* (2000)]**. Medical Linear accelerators of different manufactures available commercially, for a particular energy of electron beam striking the target, have their characteristics in terms of depth dose and lateral profile nearly in agreement with each other. However, the differences in the design and materials used for the X-ray target, flattening filter give rise to the dissimilarity in spectral characteristics of different particles contributing in the radiation beam. There are

several important applications which require the knowledge of these spectral characteristics of different type of particles, which is useful in designing of machine treatment head components and also using the linear accelerator for imaging employing megavoltage photon beams. It helps us in improving the dose delivery by intelligently altering the beam characteristics based on available spectral information. There are various experimental methods used to derive such spectra **[Nath *et al* (1976), Huang *et al* (1981), Huang *et al* (1982), Huang *et al* (1983), Lambert *et al* (1983)]** however, the difficulties are present in measuring the electron and photon energy spectra for the clinical linear accelerators. The Monte Carlo methods have proved to be the most comprehensive, accurate and easiest method of obtaining such spectra. **Few decades ago, Mohan et *al*. (1985)** provided a series of megavoltage photon beam spectra for various energies of the Varian linac using simplified models simulated in Monte Carlo technique. Due to the limited computing power available at that time their spectra suffered from statistical noise. Therefore, the purpose of our study was to develop and benchmark a Monte Carlo simulation model of 6 MV photon beam produced by Varian Clinic 600 unique performance. In this study, the validation of BEAMnrc simulated model was done by comparing the MC simulated percentage depth doses (PDDs) and beam profiles for various field sizes with the experimentally measured data. After the satisfactory validation of this simulation model, it was then used to investigate the contribution of contaminant electron to the percentage depth dose (PDD) at various depths for different field sizes. Photon spectra, photon average energy distributions, photon energy fluence spectra, contaminant electron spectra at 100 cm source to surface distance (SSD) were also computed to know the effect of these parameters on percentage depth dose.

3.2 Material & Methods

To accurately simulate the photon beam produced by linear accelerator, we must have appropriate software to model the linac head. The manufacturers do not provide the details of

electron beam hitting the X-ray target. Therefore, in this study we have used the BEAMnrc code system **[Rogers et *al.* (1995), Rogers et *al.* (2001)]** to derive best estimates for the mean energy and full width at half maximum (FWHM) of the electron beam striking the target. Monte Carlo simulations for monoenergetic beams ranging from 5.5 to 6.2 MeV with FWHM varied from 0.15 to 0.25 cm were performed to find the best match with experimentally measured PDDs and profiles data. A monoenergetic source with kinetic energy of the beam 5.7 MeV and FWHM for the X and Y directions of 0.2 cm was found to give best agreement with measured data. Geometry and materials used to build the MC simulation model of the linear accelerator were according to the specifications of machine as provided by the manufacturer Varian Medical Systems. The linac structure was organized in the following order: a target slab of tungsten and copper, primary collimator (tungsten), flattening filter, ion chamber, mirror, jaws (tungsten), and finally the option for Varian Millennium^{TM} Multileaf Collimator (MLC). All materials used in the MC simulation were extracted from the 700 ICRU PEGS4 (pre-processor for Electron Gamma Shower) cross section data accessible in BEAMnrc code. Different stages of simulation of 6 MV photon beam produced by Varian Linac using principal features of the BEAMnrc-DOSXYZnrc code **[Kawrakow et *al.* (2006) , Walters et *al.* (2005)]** are shown in figure 3.1. In the simulation of full accelerator unit we have separated the computation into three steps in order to save time. In first step, which takes a large amount of computing time, 1.5×10^7 initial histories are initiated and a monoenergetic electron beam source of kinetic energy of 5.7 MeV with FWHM for the X and Y directions of 0.2 cm was incident on the target .The primary collimator, flattening filter and ion chamber were included in this step. The output of this step is a phase space file having 7.1×10^5 number of total particles and contain the energy, position, direction, charge and history variable information for every particle exiting downstream from the end of ion chamber. Since the source and primary collimator have fixed openings, it was possible to use this phase space data

for the simulation of different field sizes. Figure 3.1(a) list the component module of BEAMnrc code used for modelling of fixed opening part of treatment head in first step. Figure 3.1(b) shows the fixed opening part modeled in BEAMnrc. This large set of particles produced in first step is used repeatedly as the input to the next step of simulations. The second step of the calculation simulates the passage of the particles through the mirror, adjustable collimator, MLC and the air slab to plane at SSD 100 cm from target. We simulated different openings of the secondary collimators system to get field sizes from 5×5 to 20×20 cm^2 at an SSD equal to 100 cm. Figure 3.1(c) list the component module of BEAMnrc code used for modelling of variable opening part of treatment head in second step of simulation. Figure 3.1(d) & (e) shows the Y and X direction view of the variable opening part of second step modeled in BEAMnrc code. We used the variable **LATCH** which allows us to store each particle's history during the first and second step of the beam simulation. Therefore, we are able to determine if a particle is scattered in the target region, primary collimator, flattening filter, adjustable collimator or MLC before reaching the scoring plane. This information was be used to calculate the various types of spectra of particles scattered by different regions. The data analysis program BEAMDP **[Ma *et al*. (1995)]** was used to analyze the phase space data files obtained at the end of second step to extract the various types of spectra of all particles reaching the plane at SSD 100 cm. In the third step of the simulations, the phase space files for field sizes of 5×5 to 20×20 cm^2 at an SSD of 100 cm were reused by the DOSXYZnrc code as an input for dose calculations in a water phantom as shown in figure 3.1 (f). We transported the particles through a water phantom of dimension 30×30×30 cm^3 with voxels size of 0.25×0.25×0.25 cm^3. The MC calculated data where compared against experimentally measured dosimetric data of 6 MV photon beam acquired using three-dimensional (3D) phantom, Blue phontom^2 IBA Dosimetry GmbH and OmniPro-Accept 7 data acquisition
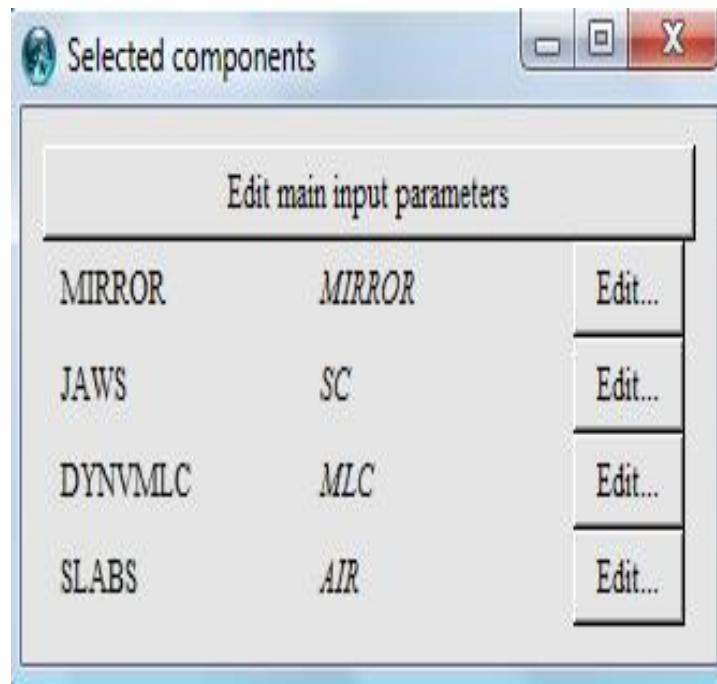
software. All the measurements were performed with a Scanditronix/ Wellhofer compact
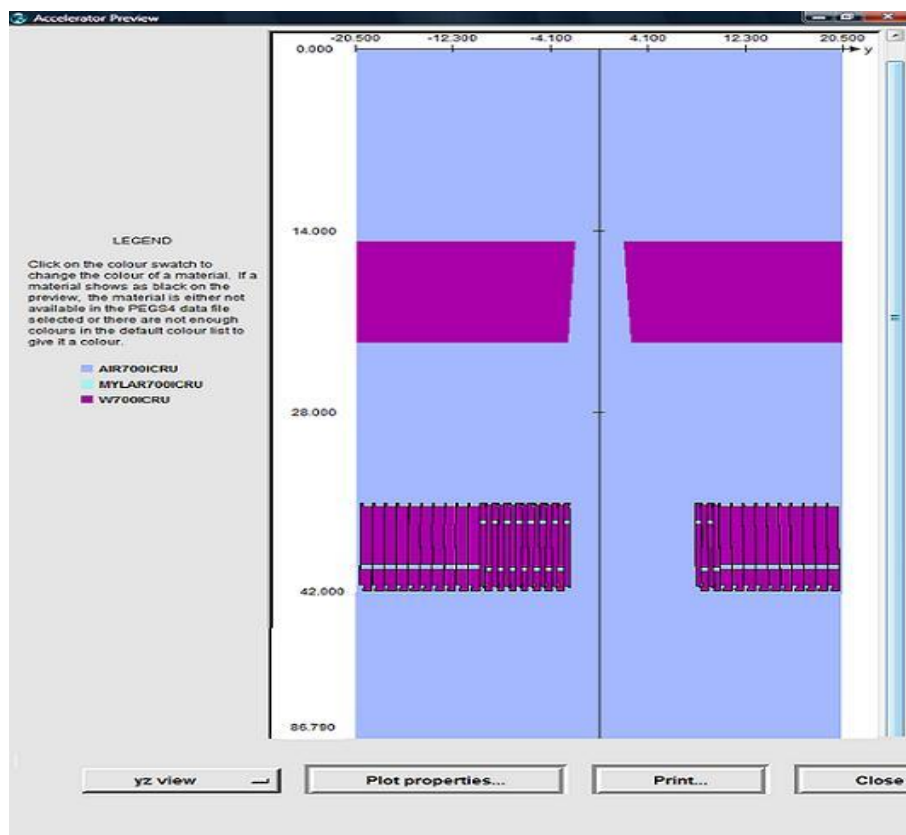ionization chamber CC13, in the water phantom.
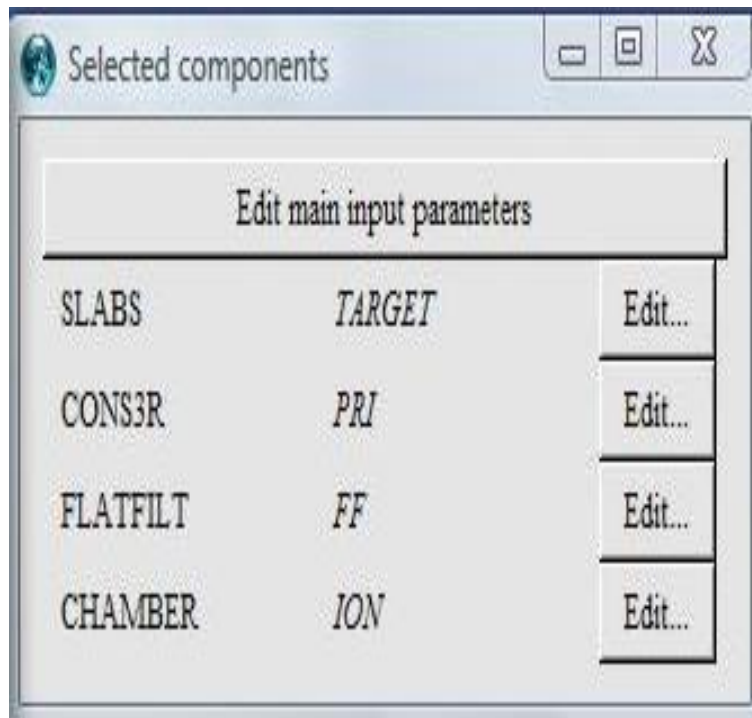
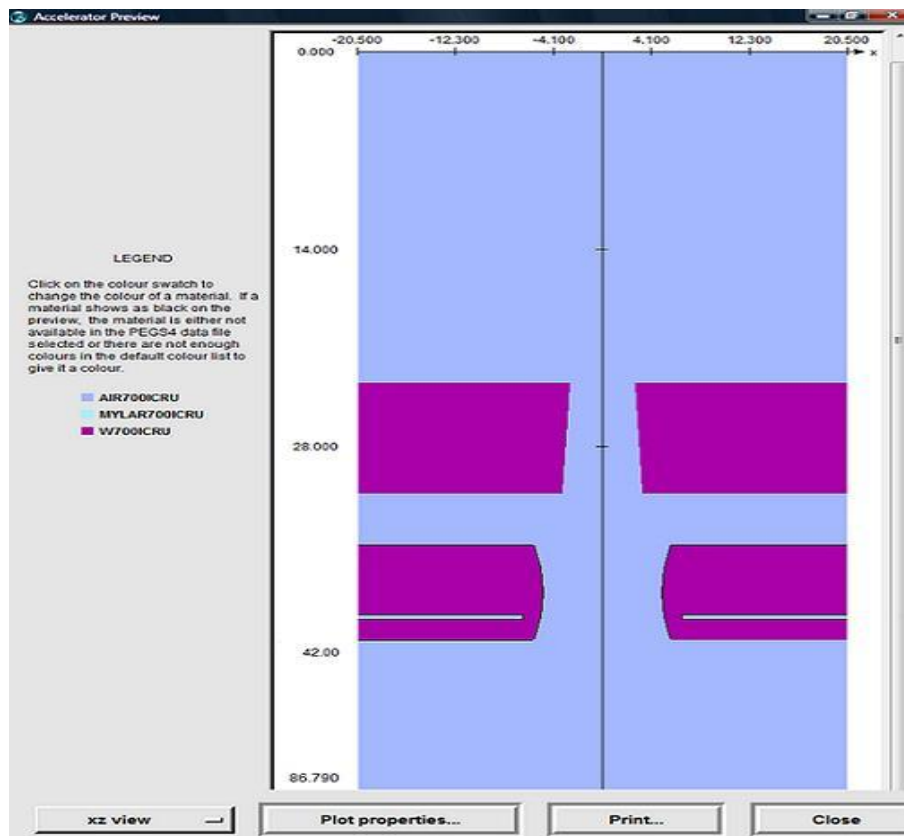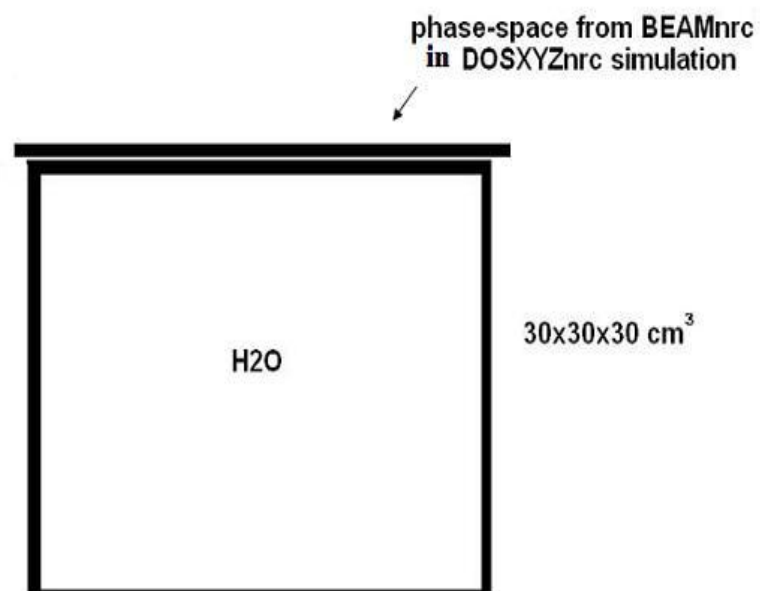**(a)**
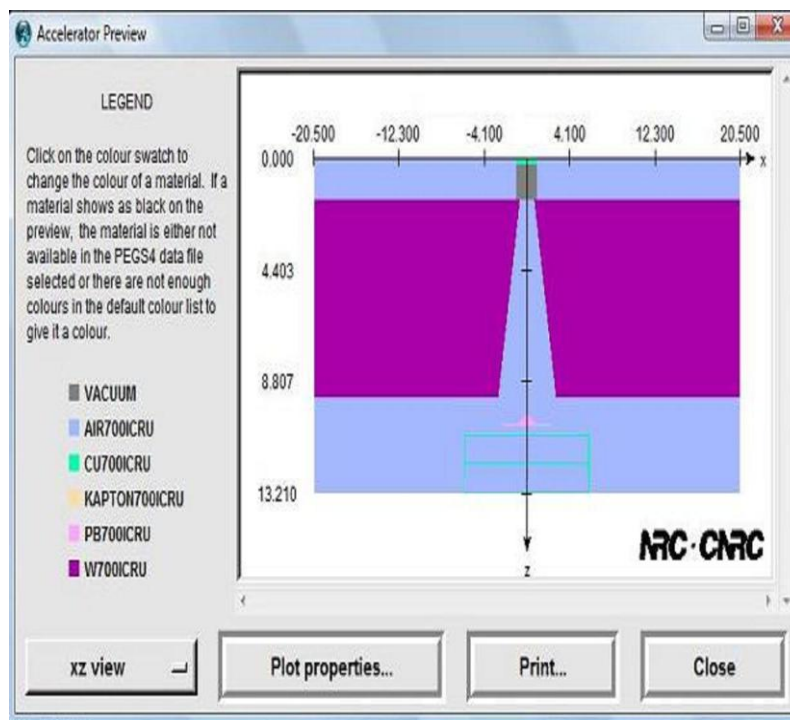
(b)

(c)

(d)

(e)

(f)

Figure 3.1 Simulation model for unique performance model of Varian Clinic 600 separated into three parts using BEAMnrc-DOSXYZnrc code **(a)** Component module used to model the treatment head fixed opening part for first step **(b)** Treatment head fixed opening part Modelled in BEAMnrc **(c)** Component module used to model the treatment head variable opening part for second step **(d)** Y direction view of treatment head variable opening part modelled in BEAMnrc showing upper jaw**(e)** X-Direction view of treatment head variable opening part modelled in BEAMnrc showing lower jaw **(f)** Dose Calculation inside water phantom in DOSXYZnrc in third step.

## 3.3 Central-axis depth-dose characteristics

3.3.1 Total Dose

Figure 3.2 show the comparison between the calculated depth-dose distributions and measurements of all the field sizes studied in this work. When comparing the simulated data with measured data. All data were normalized to the value of maximum dose on central axis. The comparison showed that the calculated and measured data agreed within 1% of local dose, and 1 mm in depth at all depths and field sizes. This excellent agreement between the calculated and measured depth-dose values showed that a good match at all depths is possible, provided that the data are measured carefully. However, statistical noise limits the size of the step (bins) used to calculate central-axis depth-dose curves using the Monte Carlo technique. Figures 3.2 also give the details of contribution of contaminant electrons to depth dose. This contribution is depicted as the percentage of maximum dose in the lower-left part and summarized in table 3.1.

3.3.2 The photon component and the electron contamination

Central-axis depth-dose characteristics for four different field sizes have been calculated in an on-axis cylinder of radius 1 cm. The total dose per incident electron on the target (Gy/inc e⁻) deposited by 6 MV photon beam on surface has been calculated by averaging the total dose deposited in the first slab of water which is 0.25 cm thick from the top of water phantom surface. The maximum dose (D_{max}) values are obtained from the bin with the maximum dose and having thickness of 0.25 cm. Dose due to photon only and electron only at surface has been calculated by averaging dose deposited in the first slab of water which is 0.25 cm thick from the top of water phantom surface. Dose due to photon only and electron only at depth of maximum dose has also been calculated.

(a)   (b)
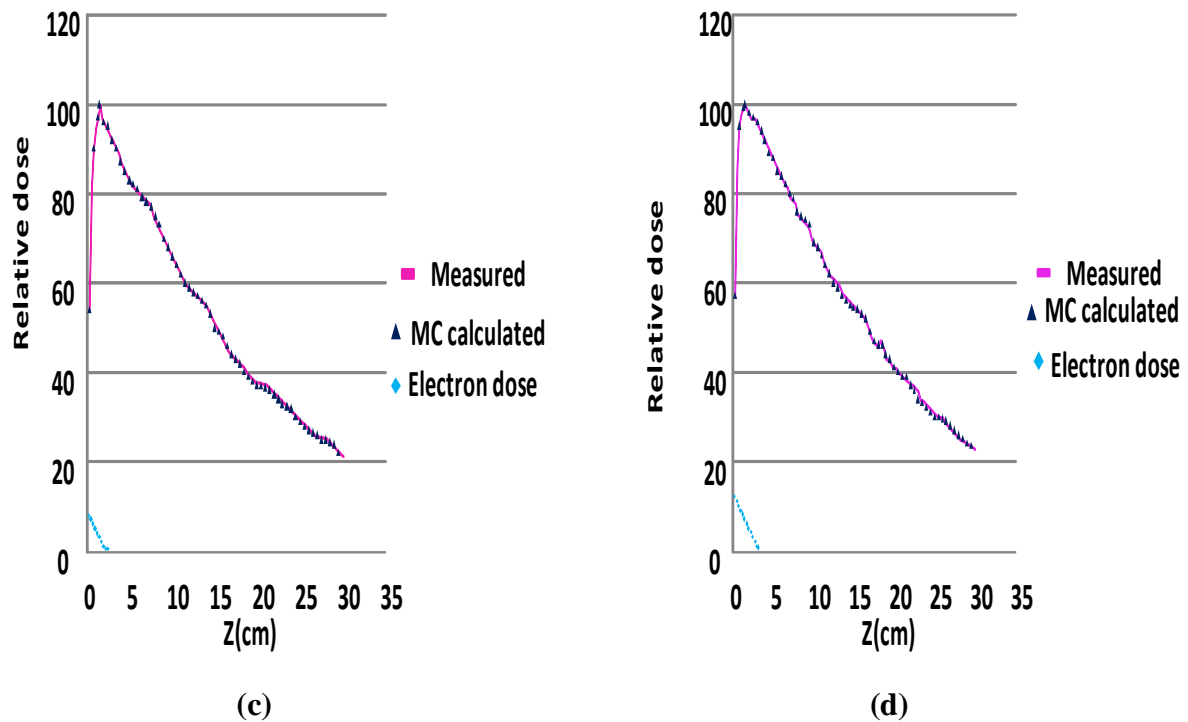
(c)

(d)
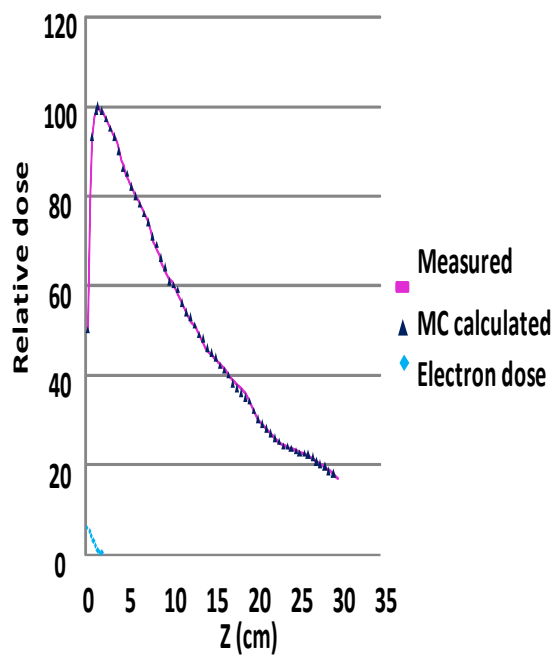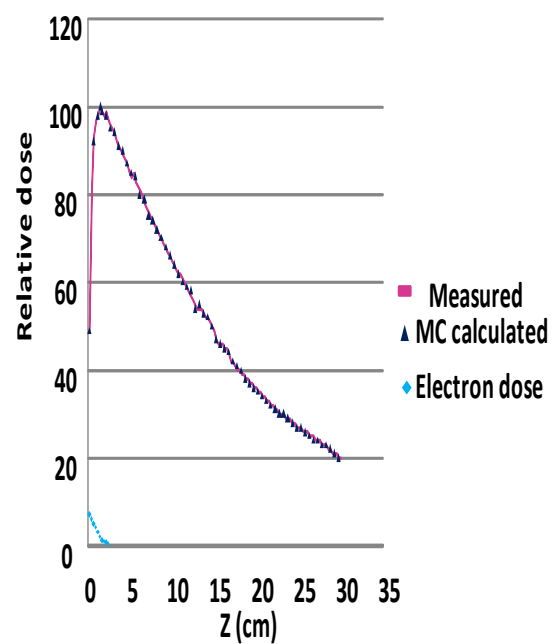
Figure 3.2 Comparison of the MC calculated and the measured central-axis depth-dose data Using a 0.2 cm FWHM, 5.7 MeV electron Beam for field size of **(a)** 5×5 cm^2 **(b)** 10×10 cm^2 **(c)** 15×15 cm^2 **(d)** 20×20 cm^2 .

Table 3.1 Central axis Depth dose calculated for on axis cylinder of radius 1 cm.

| Field Size (cm^2)	Surface dose			Dose at d$_{max}$		
	Total dose (Gy/inc e$^-$)	Dose due to photon only (Gy/inc e$^-$)	Dose due to electron only (Gy/inc e$^-$)	Total dose (Gy/inc e$^-$)	Dose due to photon only (Gy/inc e$^-$)	Dose due to electron only (Gy/inc e$^-$)
5×5	8.035×10^{-17}	6.83×10^{-17}	1.05×10^{-17}	17.63×10^{-17}	17.06×10^{-17}	0.26×10^{-17}
10×10	8.729×10^{-17}	7.38×10^{-17}	1.27×10^{-17}	18.28×10^{-17}	17.67×10^{-17}	0.49×10^{-17}
15×15	9.063×10^{-17}	7.45×10^{-17}	1.46×10^{-17}	18.78×10^{-17}	18.10×10^{-17}	0.58×10^{-17}
20×20	11.31×10^{-17}	7.53×10^{-17}	3.62×10^{-17}	20.97×10^{-17}	20.16×10^{-17}	$0 .73 \times 10^{-17}$

3.4 Profile comparison

Figure 3.3 & 3.4 shows the comparison of profiles obtained from the Monte Carlo simulation with the profiles measured experimentally at 100 cm SSD for a field size of 10×10 and 20×20 cm^2 at d_{max} (1.5cm), 5 and 10 cm depths inside the water phantom. The results were found to be within 1% of local dose, and 1 mm in depth giving satisfactory match of simulated data with experimentally measured data.
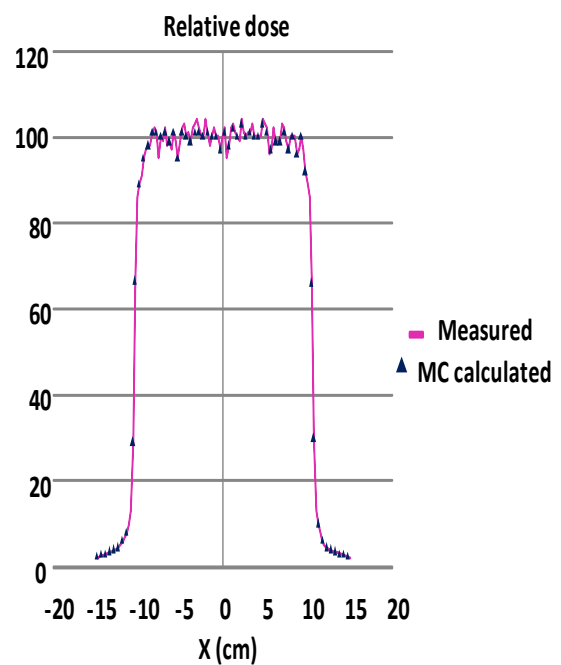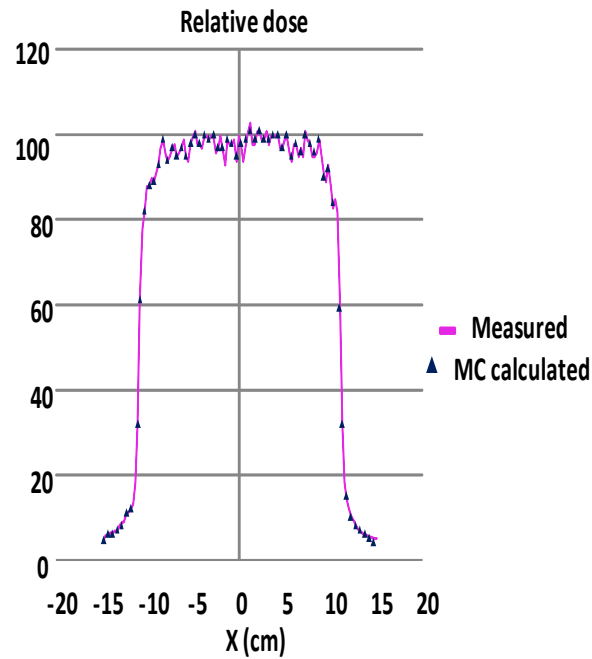

(a)   (b)
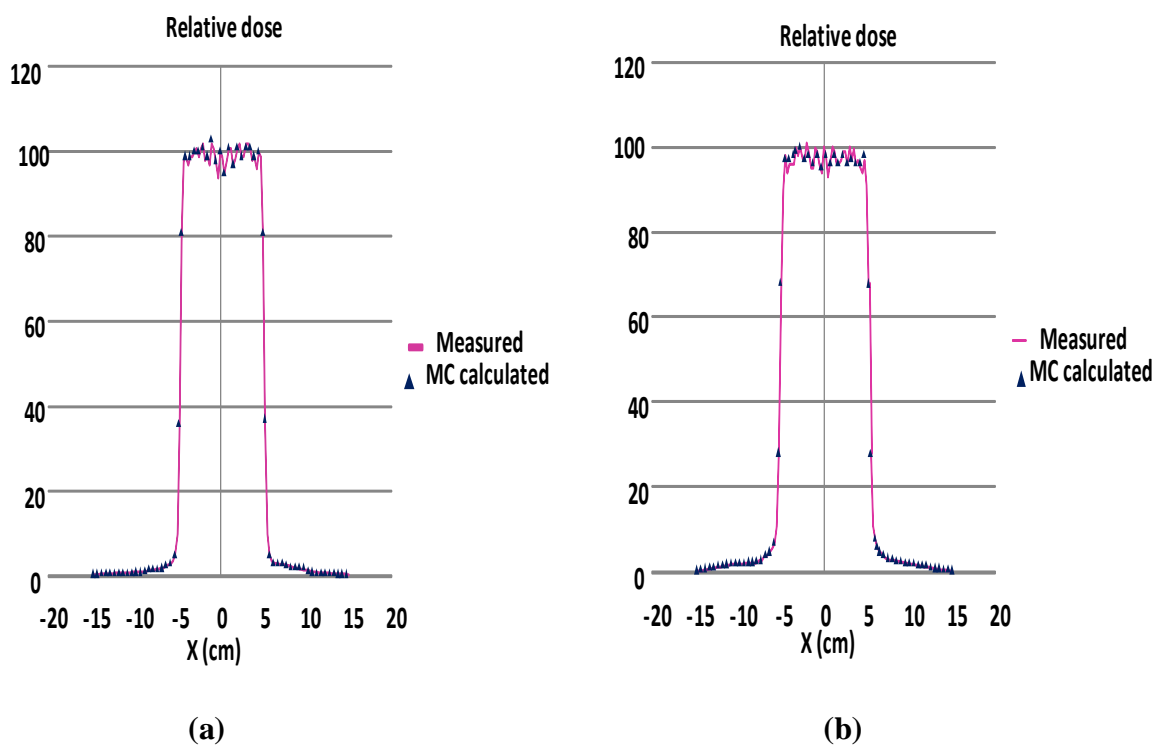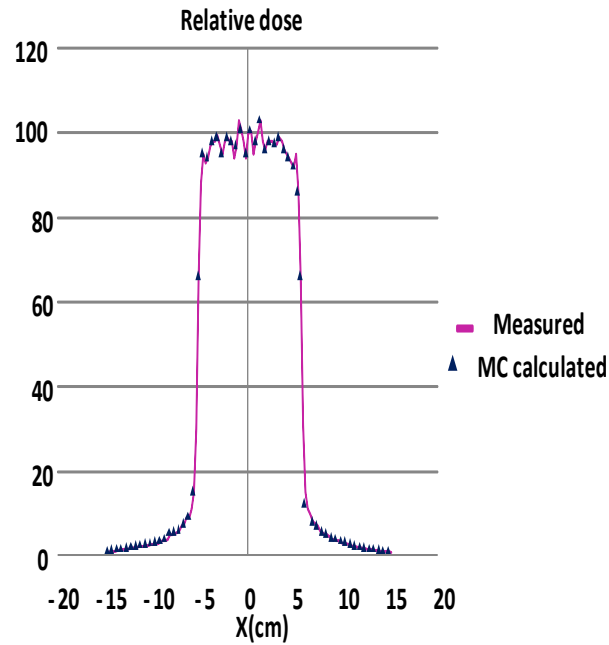
(c)

Figure 3.3 Comparison of the Monte Carlo calculated and the measured profile data for a field size of 10×10 cm^2 at depths **(a)** Z=1.5 cm **(b)** Z=5 cm **(c)** Z=10 cm .
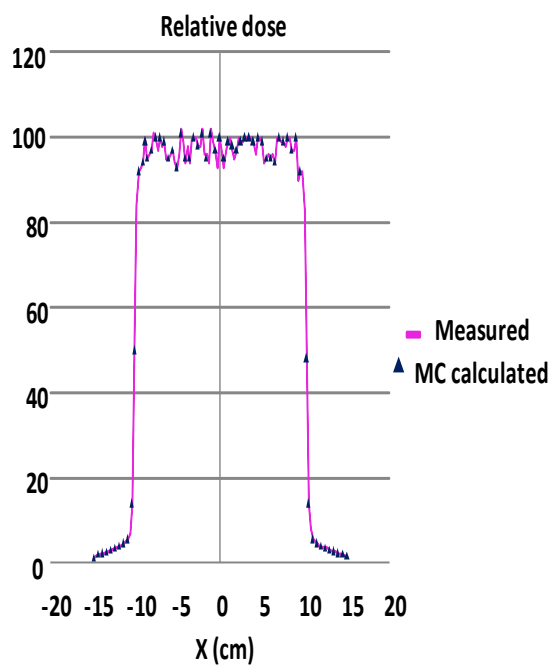
(a)

(b)

**(c)**

Figure 3.4 Comparison of the Monte Carlo calculated and the measured profile data for a field size of 20 ×20 cm^2 at depths **(a)** Z=1.5 cm **(b)** Z=5 cm **(c)** Z=10 cm .

## 3.5 Analysis of spectra

3.5.1 Photon fluence spectra

Figure 3.5 shows photon fluence spectra (number of photons per MeV per incident electron on the target) calculated for central axis. Photon emerging from target passes through the flattening filter and other components of the collimating system on their way to the scoring plain at an SSD 100 cm. Scoring plain is an annular region around the central axis with radius of 2.25 cm. The range of possible energy of Photon is divided into interval (bin) of 0.25 MeV. The number of photon within each energy bin crossing the scoring plain is being recorded and is presented in Table 3.2. The precision of calculated central-axis photon fluence spectra for all the field size used in the dose calculations is high and uncertainty in each 0.25 MeV wide bin is usually between 1 to 5%, except for the high-energy end of the spectra.
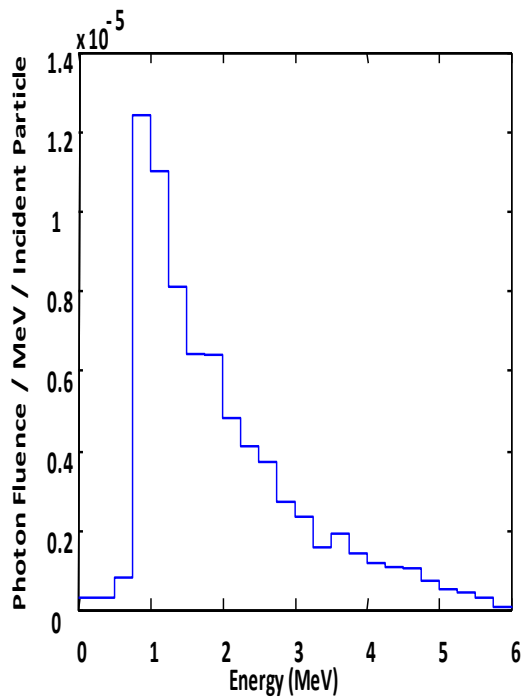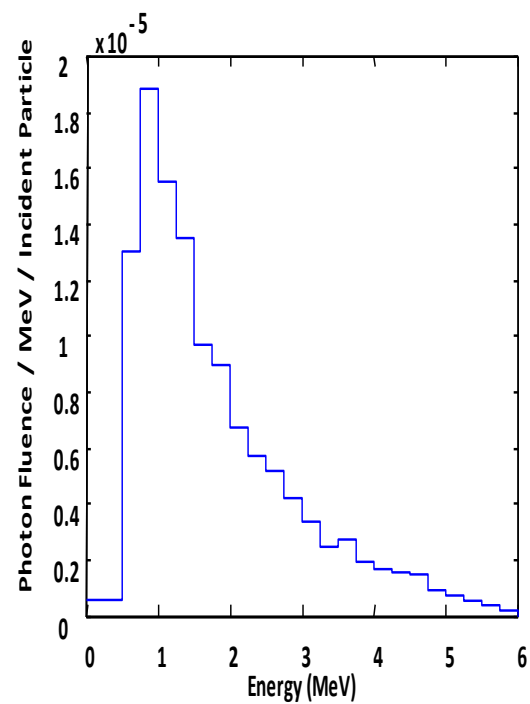
(a)
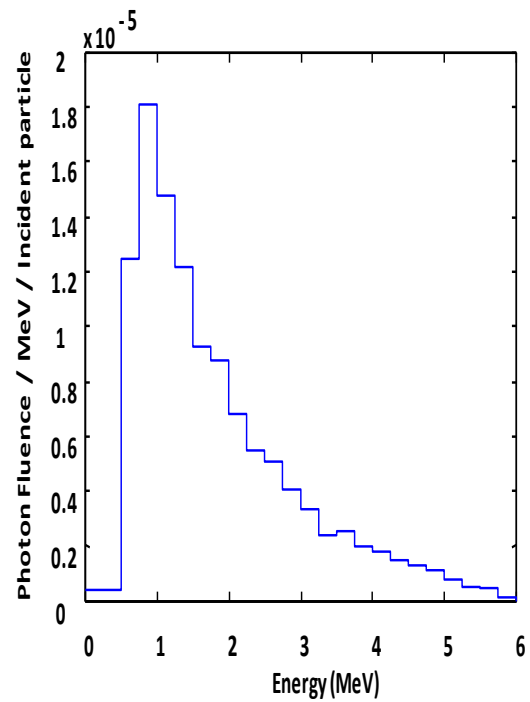
(b)
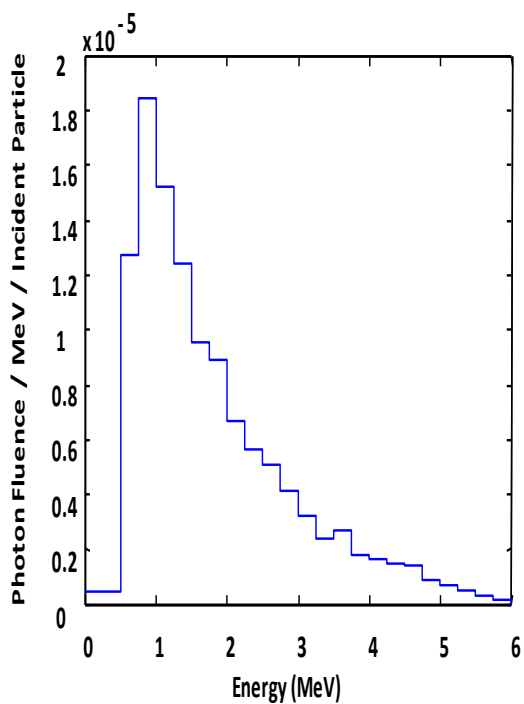
(c)

(d)

Figure 3.5 Central axis Photon fluence spectra calculated for radius 0<r<2.25 & energy bin of 0.25 MeV for field sizes of **(a)** 5×5 cm^2 **(b)** 10×10 cm^2 **(c)** 15×15 cm^2 **(d)** 20×20 cm^2 .

**Table 3. 2** Central axis photon fluence spectrum for four different field size. E stands for exponential function.

| Energy bin (MeV)	Photon Fluence spectrum for different field sizes (cm^2)			
	5×5	10×10	15×15	20×20
0.25	3.00E-007	4.41E-007	5.11E-007	6.16E-007
0.50	8.14E-007	1.25E-005	1.27E-005	1.30E-005
0.75	1.24E-005	1.81E-005	1.84E-005	1.88E-005
1.00	1.10E-005	1.48E-005	1.52E-005	1.55E-005
1.25	8.11E-006	1.22E-005	1.24E-005	1.35E-005
1.50	6.42E-006	9.30E-006	9.54E-006	9.70E-006
1.75	6.40E-006	8.81E-006	8.90E-006	9.0E-006
2.00	4.82E-006	6.85E-006	6.70E-006	6.76E-006
2.25	4.10E-006	5.52E-006	5.66E-006	5.73E-006
2.50	3.70E-006	5.10E-006	5.10E-006	5.20E-006
2.75	2.70E-006	4.08E-006	4.15E-006	4.23E-006
3.00	2.33E-006	3.38E-006	3.27E-006	3.40E-006
3.25	1.56E-006	2.44E-006	2.44E-006	2.51E-006
3.50	1.92E-006	2.57E-006	2.72E-006	2.78E-006
3.75	1.42E-006	2.01E-006	1.84E-006	1.96E-006
4.00	1.18E-006	1.84E-006	1.67E-006	1.72E-006
4.25	1.07E-006	1.53E-006	1.53E-006	1.60E-006
4.5	1.04E-006	1.35E-006	1.46E-006	1.53E-006
4.75	7.21E-007	1.13E-006	9.30E-007	9.70E-007
5.00	5.21E-007	7.91E-007	7.21E-007	7.56E-007
5.25	4.42E-007	5.46E-007	5.46E-007	5.81E-007
5.50	3.01E-007	5.12E-007	3.70E-007	4.45E-007
5.75	5.60E-008	1.61E-007	1.96E-007	2.31E-007
6.00	2.67E-008	2.71E-008	2.76E-008	3.10E-008

3.5.2 Average energy distribution

Figure 3.6(a) shows the calculated photon average energies distribution at 100 cm SSD in large open fields in annular bins as a function of off axis distance. From this figure we found that the mean photon energy was lower than generally perceived value of one third of maximum energy. Its value at central axis was 1.78 MeV and decreased to 1.3 MeV at off axis distance of 20 cm which verified that the beam hardening effect was produced by the flattening filter **[Lee *et al.* (1997)]**. The average energy distributions of total photon, direct photon and all scatter photon were plotted separately in figure 3.6. Direct photons are those which have not interacted anywhere after passing the target before reaching the scoring plane.
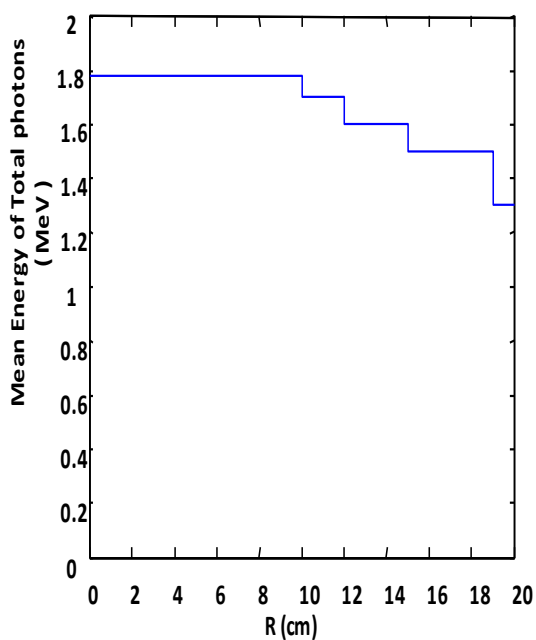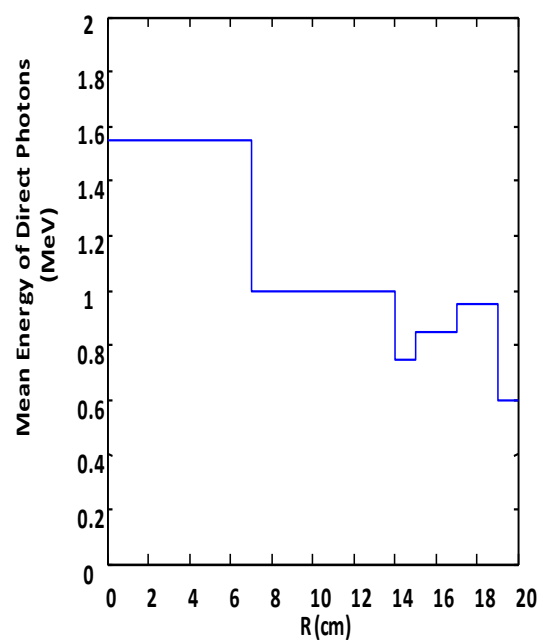
(a)   (b)
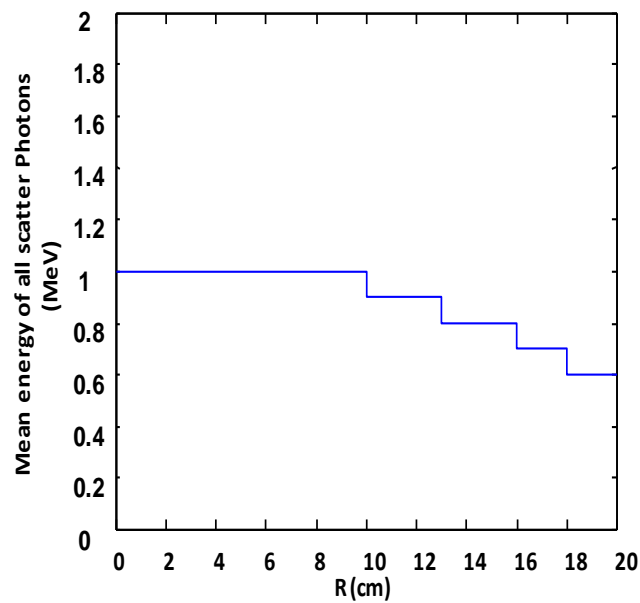
(c)

Figure 3.6 photon average energies distribution for large open fields at SSD 100 cm, scored in annular bins for **(a)** Total photon **(b)** Direct photon **(c)** all scatter photon .

3.5.3 Photon energy-fluence spectra

Figure 3.7 show the energy fluence spectra of photon for a field size of 10×10 cm^2 in contrast to the central axis photon fluence spectra (not energy-weighted) shown in figure 3.5. The energy fluence spectra of total photon, direct photon and scatter photon from Primary collimator, flattening filter, jaw were plotted separately. Direct photons are those that have only interacted in the target, before reaching the scoring plane at 100 cm SSD. The scattered photons are grouped into three major categories: those last scattered from the primary collimator, the flattening filter or the field defining jaws before reaching the scoring plane at 100 cm. The classification of photon scatter from different component modules in BEAM can be done using LATCH. The advantage of using LATCH is the simplicity of addressing a certain component module with only one number (the corresponding bit assigned to it in LATCH). We used the variable LATCH which allowed us to store each particle's history during the first and second step of the beam simulation therefore, we were able to determine

if a particle is scattered from the primary collimator, the flattening filter or the field defining jaws before reaching the scoring plane at 100 cm. This information was used to calculate the energy fluence spectra of the particles scattered by different regions. The contributions of direct and scattered photons to the total photon energy fluence for field size 10×10 cm^2 are summarized in Table 3.3. Nearly 97% of the total energy fluence was found to be due to the direct photons only and it was very difficult to find difference in total and direct energy fluence spectra. Most of the scattered photons appeared to originate from (they scatter for the last time in) the primary collimator or the flattening filter. The scatter contributions from the primary collimator and the flattening filter were found to be less than 3% of the total energy fluence while jaws were responsible for 0.25% to 0.30% of the total energy fluence. There are other structures after the target, primary collimator, flattening filter and jaws, through which the beam passes and interact with such as MLC. The scatter from these additional structures is generally much less than 1% in total, and is not explicitly depicted in figure 3.7 or Table 3.3.
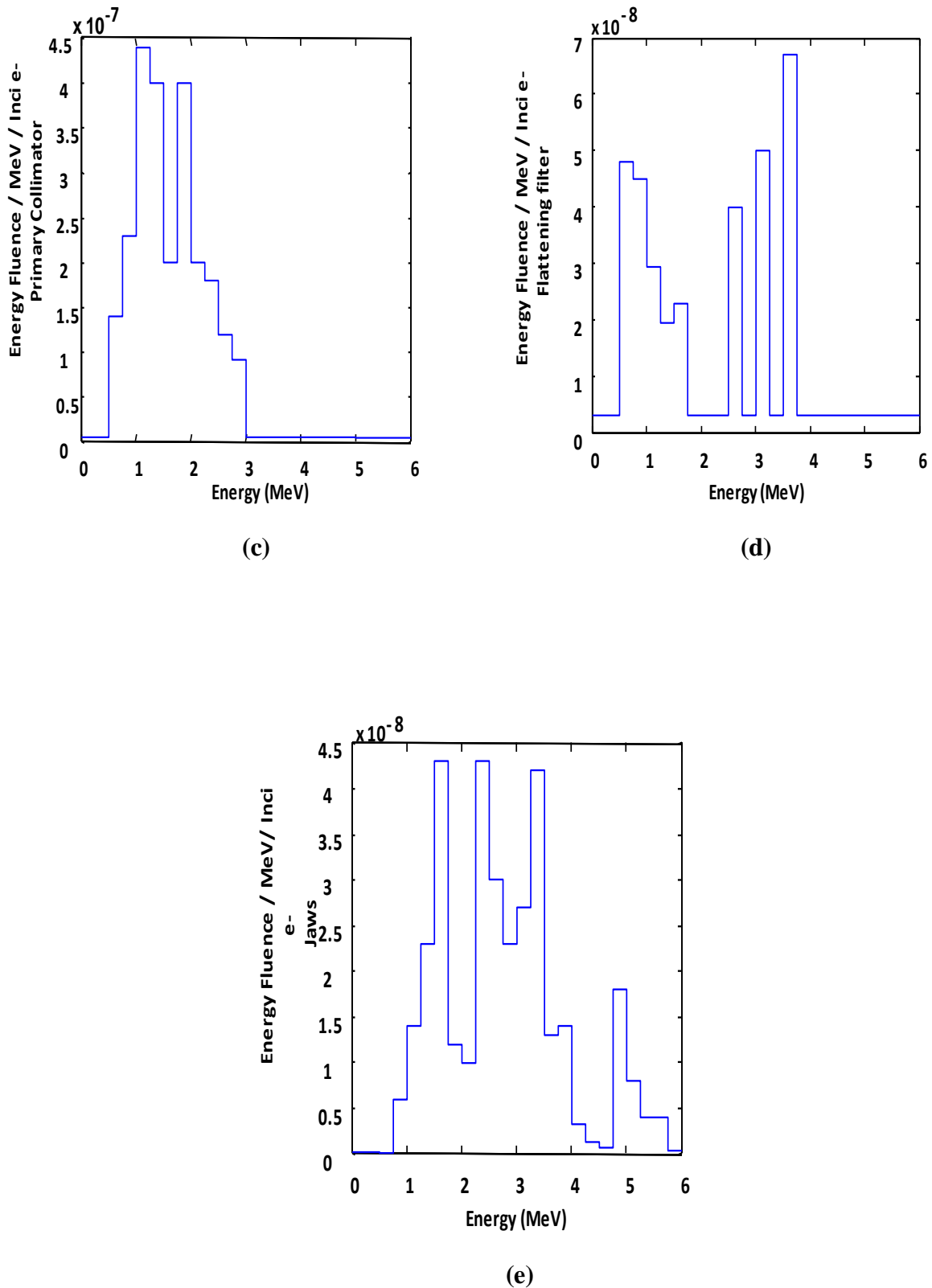

(a)   (b)

(c)

(d)

(e)
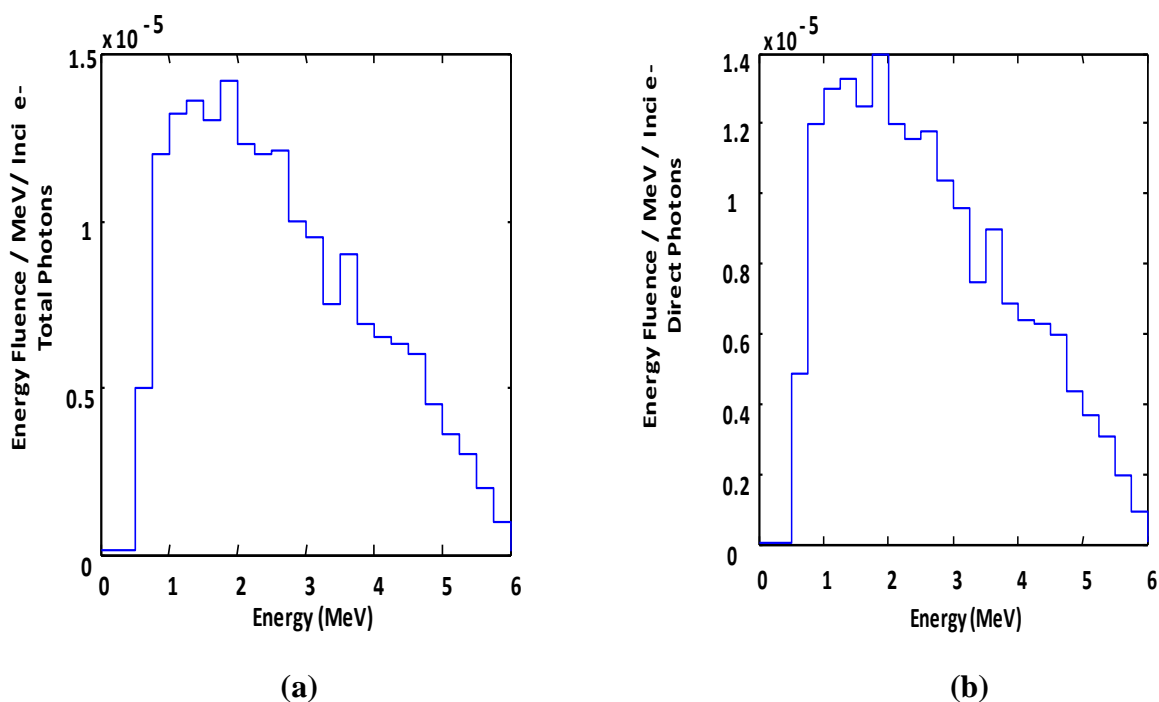
Figure 3.7 Central axis photon energy fluence spectra for a field size of 10×10 cm^2 with radius 0<r<2.25 cm & energy bin size used 0.25 MeV **(a)** Total energy fluence **(b)** Direct Photon energy fluence **(c)** Energy fluence of photon last scatter in primary collimator **(d)** Energy fluence of the Photon last scatter in flattening filter **(e)** Energy fluence of Photon last scatter in jaws.

Table 3.3 Contributions of direct and scatter photon to photon total energy fluence for a field size of 10×10 cm^2.

| Percentage of total energy fluence			
Direct	**Primary collimator**	**Flattening filter**	**Jaws**
97.0%	1.67%	0.83%	0.25%

3.5.4 Electron fluence spectra

The increase in electron fluence indicates a potential risk of delivering an elevated skin dose to the patient. Figure 3.8 shows the calculated fluence spectra for contaminant electrons calculated for central axis with radius 0<r<2.25 cm and energy bin of 0.25 MeV at 100 cm SSD for four different field size studied in this work. In our study it was found that the number of electron reaching the phantom surface strongly depends upon the field size and increases with increase in field size. The averaged value of electron fluence spectra for a field size of 20×20 cm^2 was found to be 4 times greater than its value for 5×5 cm^2.
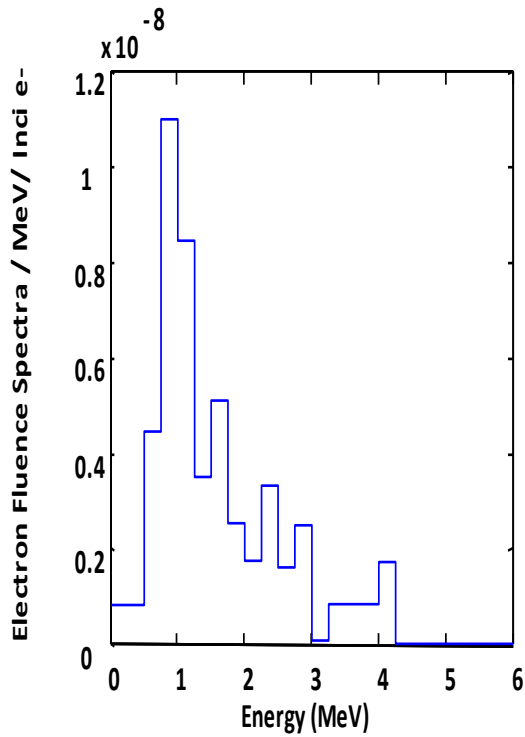
(a)
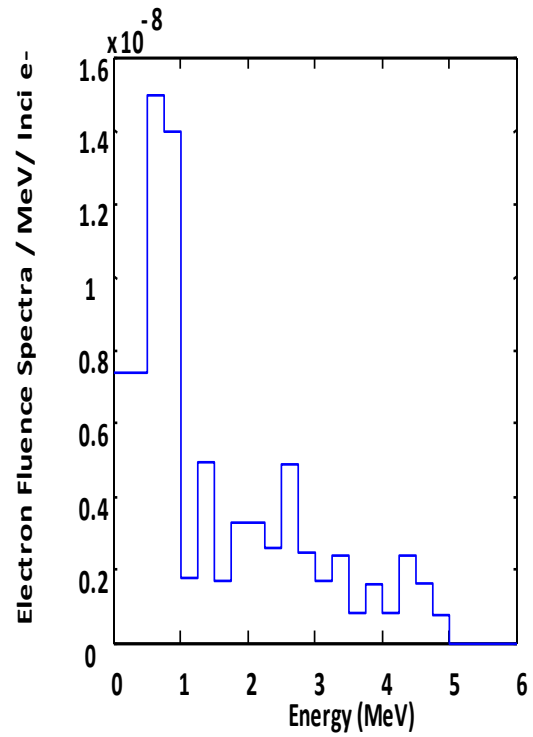
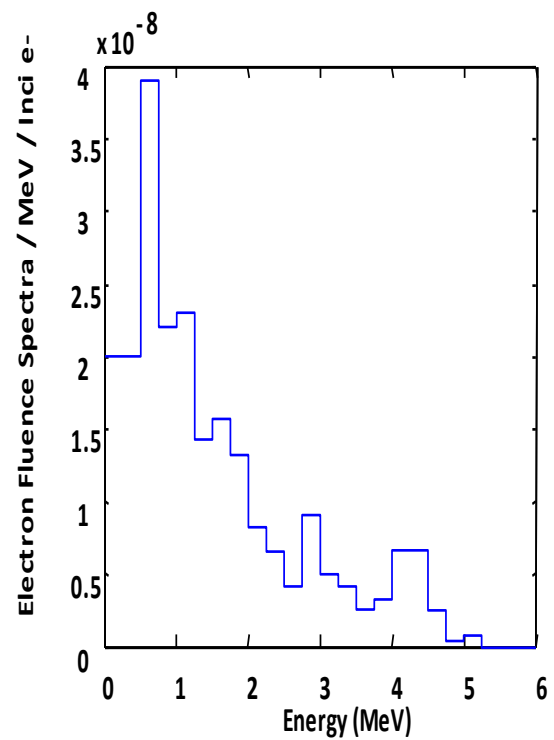**(b)**
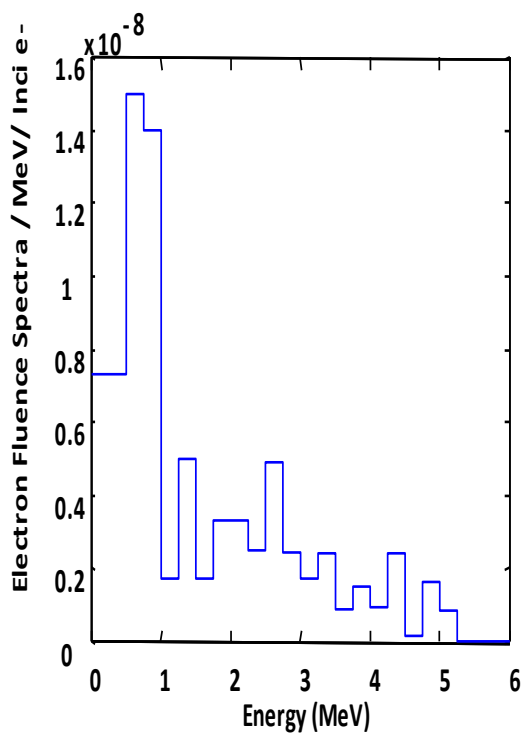
(c)

(d)

Figure 3.8 Central axis electron fluence spectrum calculated for radius 0<r<2.25 & energy bin of 0.25 MeV beam for a field sizes of **(a)** 5×5 cm^2 **(b)** 10×10 cm^2 **(c)** 15×15 cm^2 **(d)** 20×20 cm^2 .

3.6 Discussions & Conclusion

This chapter is focused on the Monte Carlo study of spectral characteristics of 6 MV photon beam and the effect of contaminant charged particles, electrons on its dosimetric properties. We have developed the accurate Monte Carlo simulation model for 6 MV photon beam produced by the Varian Clinic 600 (unique performance model) linear accelerator available at our Institute by testing and benchmarking of MC calculated data with experimentally measured percentage depth dose and profile data. The MC calculated and experimentally measured depth-dose data agreed within 1% of local dose and 1 mm in depth at all depths and field sizes which gave satisfactory validation of our Monte Carlo simulation model. Thereafter, we used this simulation model to calculate the contribution of contaminant electron to the percentage depth dose (PDDs) at various depths for different field sizes. It was observed that at the surface, contribution of electron contamination to the total dose was less than 7% of maximum total dose and at d_{max} (depth of maximum dose) it was 3% of maximum total dose for a field size of 10×10 cm^2. Therefore, with increase in depth for a given field size the contribution of electron dose to total dose decreases. Our results are in agreement with those reported by **Ding et *al.* [Ding et *al.* (2002)]** in which they showed that for 6 MV photon beam , the maximum contamination charged particle dose at the surface was 7% of maximum dose for a field size of 10×10 cm^2. The calculation made for the contribution of electron to the central-axis depth-dose for various field sizes showed that its contribution to total dose at surface increases with increase in field size. These results are comparable to the results obtained by **Butson et *al.* [Butson et *al.* (2000)]** who studied the contribution of electrons to the surface dose for a 6 MV photon beam. These results were verified with the study of on axis electron spectra at phantom surface which showed strong dependency on field size and was found to increases with increase in field size. The averaged value of electron fluence spectra for field size 20×20 cm^2 was found to be 4 times greater than the

electron fluence spectra for 5×5 cm^2 resulting in higher surface dose. Our study of photon spectra of four different field size showed that the number of photon reaching the scoring plain increases with increase in field size which also increase the amount of total dose. The photon average energy distribution as a function of off axis distance was calculated in our study. It was found that the average energy of photon decreased from 1.78 MeV on central axis to 1.3 MeV at off axis distance of 20 cm. It is due to the differential attenuation of flattening filter with increasing distance from the central axis of beam. The thick central part of the flattening filter attenuates more low energy photons, but as the off axis distance increases more low energy photons are allowed to penetrate through the thin lateral part of the flattening filter and they contribute to the photon energy spectrum, thus the mean energy of spectra is decreased. The match obtained for both average energy distribution and relative depth-dose indicate that the energy of the electron beam incident on the target to produce 6 MV photon beams, cannot be much different from 5.7 MeV used in this work. The photon energy fluence spectra were also calculated in the present study. These spectra were separated into direct and scatter components from the primary collimator, flattening filter and the adjustable collimators. About 97% of the total photon energy fluence was found to be form direct photons which have only interacted in the target, before reaching the scoring plane at 100 cm SSD. The scatter contributions to total photon energy fluence from the primary collimator and the flattening filter were typically less than 3% and jaws contribution was 0.30 % to the total photon energy fluence in the 10×10 cm^2 fields size studied. These results suggest that most of the scatter energy fluence of photon comes from flattening filter and Primary collimator. In our study we have demonstrated the use of Monte Carlo method to generate various types of spectra for photon beam. By the careful investigation of these spectra we conclude that both photon and electron fluence spectra showed strong dependency on field size and flattening filter, primary collimator are the major source of the scatter

energy fluence present in the photon beam. Thus to reduce the undesired scatter energy fluence responsible for out-of field dose delivery it is vital to investigate the effect of flattening filter on the dosimetric characteristics of photon beam which is being carried out as a major part of our thesis work and is presented in chapter 5 and 6.